catalysts

MDPI

Article

Synthesis of Novel $Zn_3V_2O_8$/Ag Nanocomposite for Efficient Photocatalytic Hydrogen Production

Fahad A. Alharthi *, Alanood Sulaiman Ababtain, Hend Khalid Aldubeikl, Hamdah S. Alanazi and Imran Hasan *

Department of Chemistry, College of Science, King Saud University, Riyadh 11451, Saudi Arabia
* Correspondence: fharthi@ksu.edu.sa (F.A.A.); iabdulateef@ksu.edu.sa (I.H.)

Abstract: In this study, we fabricated $Zn_3V_2O_8$ and a Ag-modified $Zn_3V_2O_8$ composite ($Zn_3V_2O_8$/Ag) by utilizing effective and benign approaches. Further characterization techniques such as powder X-ray diffraction (XRD) and scanning electron microscopy (SEM) were explored to examine the phase and structural properties, respectively, of the synthesized $Zn_3V_2O_8$/Ag and $Zn_3V_2O_8$/Ag composite materials. The oxidation states and elemental composition of the synthesized $Zn_3V_2O_8$/Ag and $Zn_3V_2O_8$/Ag were characterized by adopting X-ray photoelectron spectroscopy (XPS) and energy-dispersive X-ray spectroscopy (EDX). The optical band gaps of the synthesized $Zn_3V_2O_8$/Ag and $Zn_3V_2O_8$/Ag were examined by employing ultraviolet–visible (UV-vis) diffuse reflection spectroscopy. HRTEM images clearly show that ZnV@Ag NC has a hexagonal plate-like morphology. Subsequently, $Zn_3V_2O_8$ and $Zn_3V_2O_8$/Ag were used as photocatalysts for photocatalytic hydrogen (H_2) production. It was observed that after Ag doping, the energy band gap of ZnV was reduced from 2.33 eV to 2.19 eV. EDX mapping images also show the presence of Ag, O, Zn, and V elements and confirm the formation of ZnV@Ag NC with good phase purity. Observations clearly showed the presence of excellent photocatalytic properties of the synthesized photocatalyst. The $Zn_3V_2O_8$/Ag photocatalyst exhibited H_2 generation of 37.52 $\mu molg^{-1}h^{-1}$, which is higher compared to pristine $Zn_3V_2O_8$. The $Zn_3V_2O_8$/Ag photocatalyst also demonstrated excellent reusability, including decent stability. The reusability experiments suggested that ZnV@Ag NC has excellent cyclic stability for up to six cycles.

Keywords: $Zn_3V_2O_8$/Ag nanocomposite; photocatalytic H_2 production; water splitting; surface plasmon resonance; sacrificial reagents

Citation: Alharthi, F.A.; Ababtain, A.S.; Aldubeikl, H.K.; Alanazi, H.S.; Hasan, I. Synthesis of Novel $Zn_3V_2O_8$/Ag Nanocomposite for Efficient Photocatalytic Hydrogen Production. *Catalysts* **2023**, *13*, 455. https://doi.org/10.3390/catal13030455

Academic Editor: Meng Li

Received: 29 December 2022
Revised: 21 January 2023
Accepted: 8 February 2023
Published: 21 February 2023

1. Introduction

In the present scenario, the energy crisis and environmental pollution are major concerns [1–6]. Energy demand has increased drastically all over the world [4]. Energy also plays a crucial role in economic growth, progress, and development [2]. Although conventional fuels such as coal, natural gas, and oil are still regarded as the primary sources of energy, their depletion and unexpected environmental risks have prompted people to search for alternate energy sources [1]. In this context, various alternative energy technologies, such as solar cells, energy storage, and hydrogen (H_2) production, have been developed [7,8]. Various approaches and methods (electrolysis, thermolysis, and photocatalysis) have been developed for H_2 production [9]. The increasing global energy demand has directed the attention of researchers and scientists toward H_2 as a clean and green energy source for the next generations. Photocatalytic water splitting has become a hot area of research for converting cheap solar energy into hydrogen energy [10]. Photocatalytic H_2 production is an important and widely used method. In this process, the charge of a catalytic material under irradiation is transported to a counter electrode and thus initiates a redox reaction for hydrogen production [9]. PEC water splitting was first carried out by Fujishima and Honda et al. [11] at 0.8 V under ultraviolet light using a titanium dioxide

(TiO_2) photoanode, opening up a new area of study. TiO_2 has a wide band gap of 3.2 eV, which makes it unsuitable for practical PEC applications [12]. Thus, it is highly necessary to design and develop low-band-gap materials for photocatalytic H_2 production applications. According to the reported literature, a suitable photocatalyst should have a narrow band gap for better charge transfer during the photocatalytic process [13,14]. It has also been noted in the available literature on photocatalytic H_2 evolution that surface properties such as morphological characteristics largely influence the H_2 evolution rate and photocatalytic H_2 evolution by providing a better path for electron transport [14]. Thus, it is noted that the mechanical stability, surface structural properties, and band gap of the photocatalyst can have a direct influence on the H_2 evolution rate [15]. Nanostructured photocatalysts can easily separate electron–hole pairs during a photocatalytic reaction and may generate a suitable and easy path for electron transport, which can significantly enhance the photocatalytic H_2 evolution [9]. Recently, various novel photocatalyst materials with unique and nanostructured surface morphologies have been widely used for photocatalytic H_2 evolution reactions [10]. In this context, TiO_2, zinc oxide, molybdenum disulfide, cadmium sulfide, and graphite-like carbon nitride materials have been widely used for H_2 production [6,9,10]. Although various nanostructured materials have been reported for the H_2 evolution process, there is still room for the design and fabrication of novel photocatalysts for the H_2 evolution process.

In the past few years, metal vanadates have received extensive attention because of their exceptional charge transport/separation and optical properties [13–16]. Additionally, metal vanadates have band gaps of 2.2 to 2.7 eV, which enables them to effectively absorb solar energy in the visible range [17–19]. Moreover, metal vanadates are relatively robust against photocorrosion [20]. In addition, the valence band location is close to the thermodynamic potential of oxygen evolution, making them good catalysts for the visible-range photo-oxidation of water [21]. Zinc vanadate ($Zn_3V_2O_8$) has excellent optoelectronic features and has been extensively used in supercapacitors, batteries, H_2 storage, catalysis, photocatalysis, and magnetic devices [22–25]. However, there are still some challenges that limit their photocatalytic efficiency, such as the minimum energy band gap needed to break water into hydrogen and oxygen, as most semiconductors have wider band gaps. Secondly, the electron–hole recombination rate hinders the light absorption of the semiconductor material, and hence, low photocatalytic efficiency is achieved [19,23,24]. To overcome these barriers, several procedures and efforts have been reported, and out of these, merging the properties of two different materials is of great significance for a variety of applications [26]. Thus, it is worth designing and fabricating hybrid composite materials containing $Zn_3V_2O_8$. Silver nanoparticles (Ag NPs) possess excellent catalytic and conducting properties [27]. Ag NPs have been widely used for the preparation of hybrid composite materials [28].

There are very few reports available on metal-vanadate-based photocatalytic H_2 production. Very low hydrogen production of 11.5 $\mu molg^{-1}h^{-1}$ was reported for a bismuth vanadate-modified reduced graphene oxide composite ($BiVO_4$/rGO) [18]. Another work also demonstrated the use of $BiVO_4$/rGO as a photocatalyst for improved H_2O_2 evolution [14]. Thus, it is revealed that metal vanadate has excellent properties and can be explored in the photocatalytic H_2 evolution process.

In this study, our group successfully fabricated a Ag-NP-decorated $Zn_3V_2O_8$ composite material. Furthermore, photocatalytic H_2 production studies were carried out using the $Zn_3V_2O_8$/Ag NP composite. The investigations demonstrated reasonable improvements in the photocatalytic activity of the $Zn_3V_2O_8$/Ag NP composite compared to pristine $Zn_3V_2O_8$. According to our literature survey, we report for the first time the photocatalytic activity of a $Zn_3V_2O_8$/Ag NP composite for H_2 production applications. In the present study, we propose a simple synthetic strategy for the preparation of a $Zn_3V_2O_8$/Ag NP composite and explored it as a cost-effective, environmentally friendly, highly stable, and efficient photocatalyst for H_2 production applications.

2. Results and Discussion

2.1. Materials Characterization

The XRD patterns of ZnV and ZnV@Ag NC were obtained in the 2θ range of 10–100°. The obtained XRD data of ZnV and ZnV@Ag NC are displayed in Figure 1. The XD pattern of ZnV shows various diffraction peaks at 2θ values of 10–100°. The obtained diffraction peaks can be assigned to the well-defined (001), (010), (002), (110), (012), (111), (020), (021), (112), (013), (022), (023), (122), (220), and (021) diffraction planes of ZnV. The XRD pattern is in agreement with the reported JCPDS number of 50-0570. The strong diffraction peaks indicate that ZnV has decent crystallinity. The XRD pattern of ZnV@Ag NC demonstrates the presence of (002), (110), (012), (020), (021), (013), (122), and (024) diffraction planes. No diffraction plane or peak was observed for Ag NPs, which is due to the low amount of Ag NPs in the synthesized ZnV@Ag NC sample. Further information about the crystallite size can be obtained by using the Debye–Scherer formula given by Equation (1) [29]:

$$D_c = \frac{K\lambda}{\beta \times Cos\theta} \quad (1)$$

where λ is the wavelength of the X-ray source, K is a shape factor and is usually ~0.9, θ is the corresponding angle, and β is the breadth of the observed diffraction line at its half-intensity maximum. Using Equation (1), the crystallite sizes of ZnV and ZnV@Ag were found to be 27.50 nm and 24.60 nm. The overall XRD results confirmed that ZnV and ZnV@Ag NC are formed with decent phase purity. The crystallite sizes of the synthesized ZnV and ZnV@Ag NC are presented in Table 1. The observations showed that the insertion of Ag reduced the crystallite size of ZnV@Ag NC.

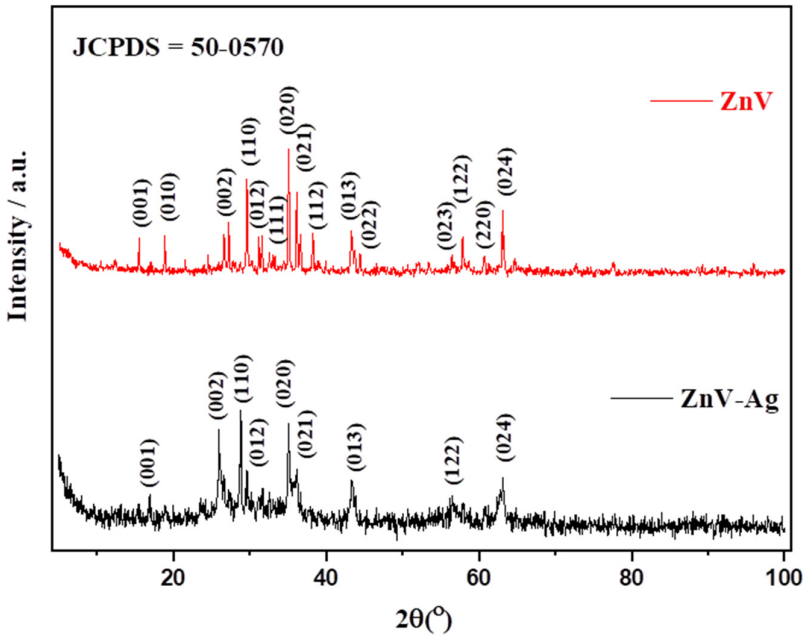

Figure 1. XRD data of ZnV and ZnV-Ag NC.

The FTIR spectra of the prepared ZnV and ZnV@Ag NC were collected to further authenticate the formation of ZnV and ZnV@Ag NC. Figure 2 shows the FTIR spectra of ZnV and ZnV-Ag NC. The FTIR spectrum of ZnV shows absorption bands at 417 and 498 cm^{-1}, which are related to the vibration and stretching modes of Zn-O bonds [30]. The presence of vibrational peaks at 838, 648, and 793 cm^{-1} is attributed to the presence of tetrahedral VO_4 vibrational modes and asymmetric vibration modes of V-O-Zn and V-O-V in the ZnV sample [30,31]. The FTIR spectrum of ZnV@Ag shows an absorption band at 415 cm^{-1}, which can be ascribed to the Zn-O bond [30]. Similarly, the presence of

vibrational peaks at 823, 637, and 782 cm^{-1} are attributed to the presence of tetrahedral VO_4 vibrational modes and asymmetric vibration modes of V-O-Zn and V-O-V in the ZnV sample [31]. The observed results indicate that the presence of Ag NPs in the ZnV@Ag sample slightly shifted the absorption band positions. The obtained results are similar to those in a previous report [31].

Table 1. XRD parameters such as crystallite size, lattice parameters, unit volume, and band-gap energy for ZnV and ZnV@Ag NC.

Material	Crystallite Size (nm)	Lattice Parameters	Unit Volume	Energy Band Gap
ZnV	27.50	a = 6.18 Å, b = 11.76 Å, c = 8.38 Å	609.03 $Å^3$	2.33 eV
ZnV@Ag	24.60	a = 5.88 Å, b = 11.38 Å, c = 8.18 Å	547.97 $Å^3$	2.19 eV

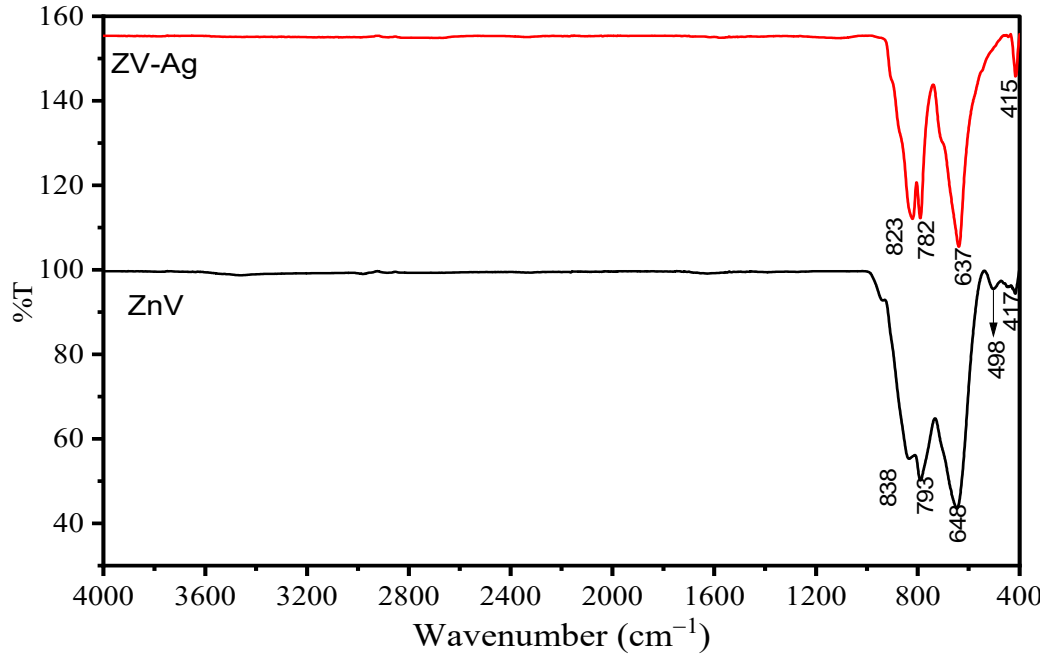

Figure 2. FTIR of ZnV (black line) and ZnV@Ag NC (red line).

The topological and surface structural features of ZnV and ZnV@Ag NC were studied by obtaining their SEM images. The obtained SEM results for ZnV and ZnV@Ag NC are provided in Figure 3. From the SEM investigations, it was observed that a plate-like surface with a uniform particle distribution was formed. Some particles were agglomerated and interconnected (Figure 3a). The average particle size of ZnV was less than 100 nm (Figure 3a). In further investigations, SEM pictures of ZnV@Ag NC were also recorded under the microscope. Figure 3b shows that Ag nanoparticles are embedded in the surface of the ZnV photocatalyst. The Ag particles have a thin needle-like surface morphology and are very well connected to the ZnV surface, as shown in Figure 3b.

Further, the presence of Ag on the ZnV surface was confirmed by the EDX study. The recorded EDX spectrum of ZnV@Ag NC is presented in Figure 3c. The EDX results for ZnV@Ag NC revealed the presence of Ag, O, Zn, and V elements. This further verified that Ag NPs had been successfully grown on the ZnV surface. EDX mapping images of ZnV@Ag NC were also obtained and are displayed in Figure 4a–e. The EDX mapping images also show the presence of Ag, O, Zn, and V elements and confirm the formation of ZnV@Ag NC with good phase purity.

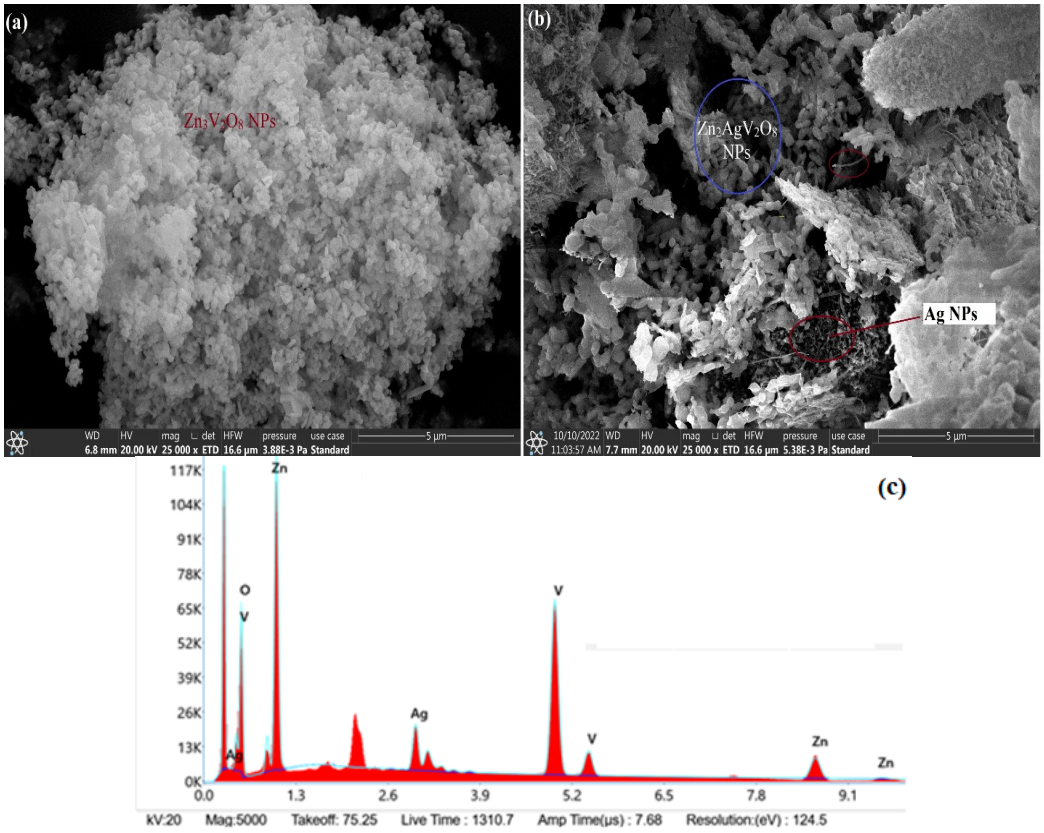

Figure 3. SEM images of ZnV (**a**) and ZnV@Ag NC (**b**) and EDX spectrum of ZnV@Ag NC (**c**).

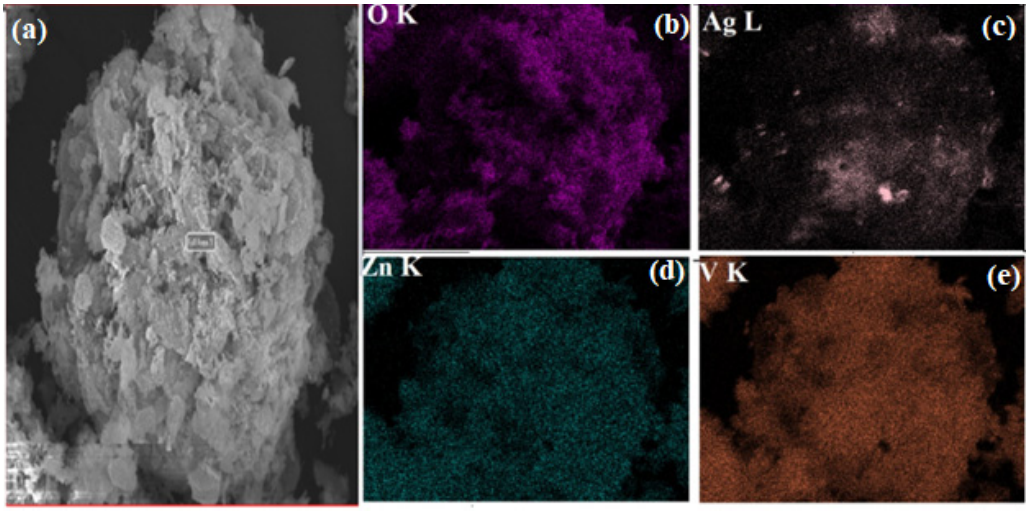

Figure 4. Selected-area SEM image (**a**) and mapping images of O (**b**), Ag (**c**), Zn (**d**), and V (**e**) elements present in ZnV@Ag NC.

Furthermore, TEM analysis was also conducted to further identify the structural properties of the prepared ZnV@Ag NC. The obtained TEM results for ZnV@Ag NC are presented in Figure 5. Figure 5a shows that Ag NPs are present on the ZnV surface with particle sizes less than 100 nm. The high-resolution TEM image is displayed in Figure 5b. The HRTEM image clearly shows that ZnV@Ag NC has a hexagonal plate-like morphology.

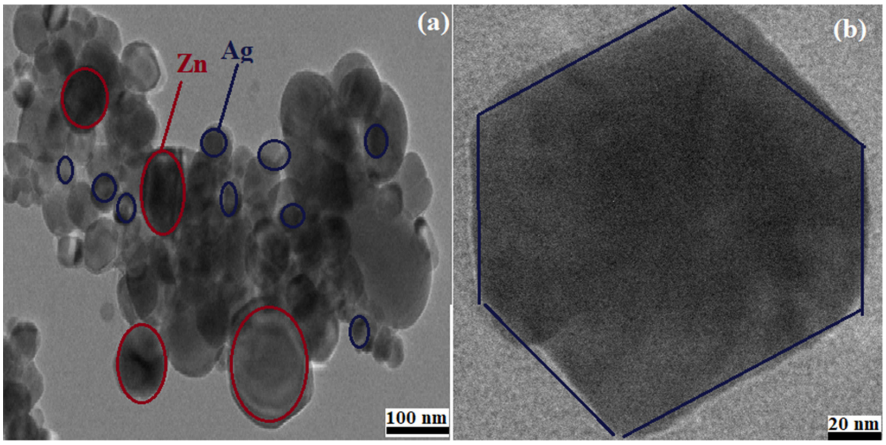

Figure 5. (**a**) TEM image of ZnV@Ag NC. (**b**) High-resolution TEM image of ZnV@Ag NC.

We can conclude that Ag NPs were successfully grown on the hexagonal plate-like surface of ZnV. The UV-vis reflectance spectra of ZnV and ZnV@Ag NC are presented in Figure 6a. The UV spectra of ZnV exhibited two peaks at 288 nm and 393 nm. The 288 nm peak is attributed to the transfer of charge from oxygen to the central metal V atom, while 393 nm is due to the transfer of charge from oxygen to the zinc atom [32,33]. The UV spectrum of ZnV@Ag exhibited the same type of pattern with an extra peak at 480 nm associated with Ag coordinated with an oxygen atom [34]. The reflectance curve for ZnV@Ag NC was found to have higher reflectance in the visible region as compared to pristine ZnV NPs due to the surface plasmon resonance (SPR) effect of doped Ag NPs. The SPR effect generally arises in metal nanoparticles due to collective oscillations of free electronic charge under the influence of electromagnetic radiation [35]. The SPR effect is generally affected by the particle size, size distribution, and shape of the particle in a particular medium. The doping of Ag in ZnV results in the origination of the SPR effect in the material, which partially contributed to the enhancement of photocatalytic activity by reducing the electron–hole pair recombination rate [36]. The band gaps of ZnV and ZnV@Ag NC were determined by extrapolating the linear portion of the $(F(R)hv)^2$ curve versus the photon energy (hv) using the Kubelka–Munk equation, which is given by Equation (2) [37]:

$$(F(R)h\upsilon) = A(h\upsilon - Eg)^n \quad (2)$$

where R is diffused reflectance, h is the Planck constant, υ is the frequency of radiation, A is a constant, Eg is the energy band gap, and n is an integer measuring the magnitude of direct and indirect energy band gaps. The synthesized ZnV and ZnV@Ag NC show band gaps of 2.33 and 2.19 eV, respectively. The observed results show that the presence of Ag reduced the band gap of ZnV, which makes it a more suitable candidate for photocatalytic applications.

Furthermore, we also used the XPS technique to identify the existence of the valence state of Ag in the synthesized ZnV@Ag sample. The XPS survey scan of ZnV@Ag NC is shown in Figure 7a. The survey spectrum of ZnV@Ag shows the presence of Ag3d, V2p, Zn2p, and O1s, which suggested that ZnV@Ag had been formed. The presence of binding energies at ~1023 eV and 1046 eV is attributed to $Zn2p_{3/2}$ and $Zn2p_{1/2}$ of Zn^{2+}, respectively (Figure 7b). According to the high-resolution V2p spectrum, the appearance of two peaks at binding energy values of 522.5 and 515.7 eV can be ascribed to $V2p_{5/2}$ and $V2p_{3/2}$ of V^{5+} in ZnV, respectively (Figure 7c). The presence of two peaks at binding energies of 365.4 and 372.4 eV can be assigned to $Ag3d_{5/2}$ and $Ag3d_{3/2}$, respectively (Figure 7d). The obtained high-resolution XPS spectrum of Ag3d suggested the presence of metallic Ag (0). Figure 7e shows the O1s spectrum of ZnV@Ag, and the presence of a peak at the binding energy value of 528.34 eV can be assigned to the presence of lattice oxygen in the ZnV@Ag sample. The XPS results for ZnV@Ag are well matched with the published literature [31].

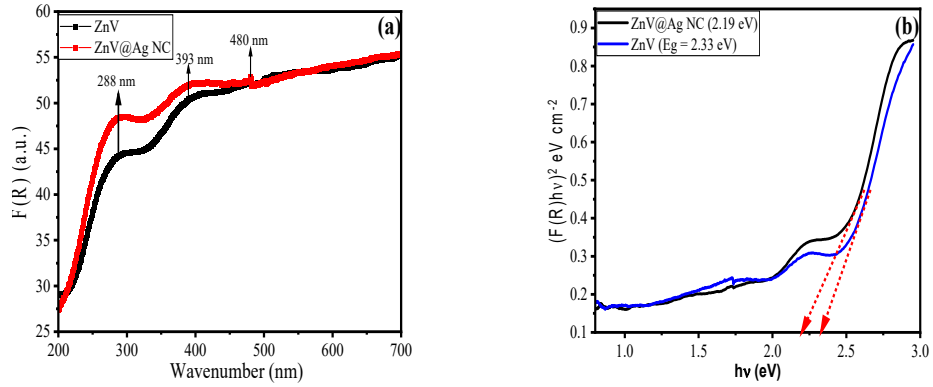

Figure 6. UV-vis reflectance spectra (**a**) and band-gap plot (**b**) of ZnV and ZnV@Ag NC.

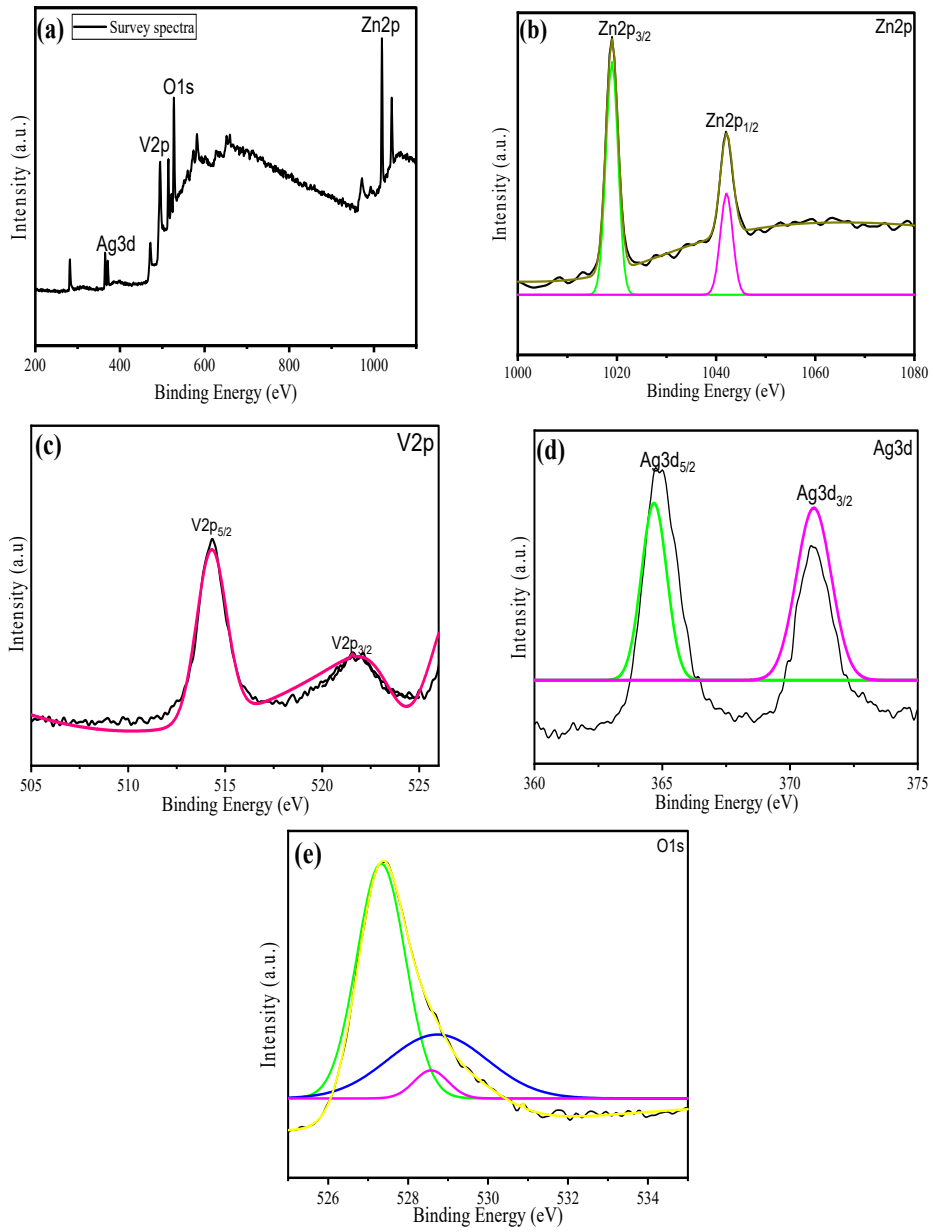

Figure 7. XPS survey spectrum of ZnV@Ag NC: (**a**) Zn2P (**b**), V2p (**c**), Ag3d (**d**), and O1s (**e**) of ZnV@Ag.

2.2. Photocatalytic H_2 Production Activities

The photocatalytic activities of the prepared ZnV and ZnV@Ag NC photocatalysts were studied in the presence of lactic acid. The obtained results are presented in Figure 8a. The ZnV photocatalyst exhibits good photocatalytic activity toward H_2 generation, and a reasonably good amount (16.44 $\mu molg^{-1}h^{-1}$) was obtained. Further studies showed interesting photocatalytic properties of ZnV@Ag NC for H_2 generation. The improved H_2 generation amount of 37.52 $\mu molg^{-1}h^{-1}$ was obtained for ZnV@Ag NC. This suggests that ZnV@Ag NC has excellent photocatalytic properties, which may be ascribed to the narrow band gap and synergistic interactions between Ag NPs and ZnV. In the above studies, the pH of the solution was 3. Since pH may significantly alter the performance of the photocatalyst, we further checked the effect of various pH values on photocatalytic H_2 generation. The optimal photocatalytic performance of ZnV and ZnV@Ag NC was found at pH 3. The lowest H_2 generation was observed at pH 7 (Figure 8b). The optimized pH of 3 was utilized for further experiments. The type of solvent may play a vital role in activating the photocatalyst. Thus, the photocatalytic activities of the prepared ZnV and ZnV@Ag NC photocatalysts were examined in the presence of various solvents: water, methanol, lactic acid, Na_2S/Na_2SO_3, and triethanolamine. The observations indicate that ZnV and ZnV@Ag NC have poor photocatalytic activities in water. This activity was slightly enhanced when water was replaced with triethanolamine. Further enhancements were observed for methanol- and Na_2S/Na_2SO_{30}-based systems. However, the highest photocatalytic activities of ZnV and ZnV@Ag NC were observed in lactic acid compared to the other solvents (Figure 8c). The amount of photocatalyst affects its performance; thus, we optimized the amount of the photocatalyst for improved H_2 generation.

Various amounts (10, 20, 30, 40, 50, 60, 70, 80, 90, and 100 mg) of ZnV and ZnV@Ag NC photocatalysts were used to optimize the photocatalytic performance for effective H_2 generation in lactic acid. The obtained data are summarized in Figure 8d. The obtained results revealed that 60 mg of the photocatalyst has the most effective and efficient photocatalytic performance (Figure 8d). The amount of lactic acid was also optimized, and the obtained results are depicted in Figure 8e. The highest amount of H_2 was produced in the presence of 25 mL of lactic acid, as shown in Figure 8e. The above investigations demonstrated excellent photocatalytic activities of ZnV@Ag NC, which suggests its potential applications at a large scale. It is believed that a photocatalyst should have excellent stability or reusability for H_2 production. In this context, we examined the reusability of ZnV@Ag NC in the presence of 25 mL of lactic acid. The obtained results are displayed in Figure 8f. It can be clearly observed that ZnV@Ag NC has excellent cyclic stability for up to 6 cycles.

The obtained H_2 production activities of ZnV and ZnV@Ag NC are summarized in Table 2.

2.3. Mechanism of H_2 Production

Scheme 1 presents the plausible mechanism for the water-splitting and lactic acid oxidation/reforming reaction over ZnV@Ag NC under visible-light irradiation. When the material is placed under the light, the formation of electron–hole pairs occurs (Equation (3)). The photogenerated electrons can move from the conduction band (CB) of ZnV to Ag metal via the SPR effect and thereby get trapped, thus hindering electron–hole recombination. The photogenerated holes in the valence band (VB) interact with water to form H^+ and $^{\bullet}OH$ radicals (Equation (4)). The H^+ ions are reduced to H_2 gas on the metal surface (Equation (5)), while the $^{\bullet}OH$ radicals react with lactic acid to further produce H^+ ions and other oxidized products. The oxidized products further degrade to form CO_2 and H_2O (Equation (6)), and H^+ ions are reduced to produce H_2 gas on the catalyst surface. Thus, the sacrificial reagent lactic acid performs a dual role as a H+ ion producer and a suppressor of

the electron–hole pair recombination rate by reacting with hydroxyl radicals and stabilizing the photogenerated holes, hence increasing the hydrogen production efficiency [38,39].

$$ZnV@Ag \xrightarrow{h\upsilon} ZnV@Ag^{*}(h^{+}_{VB} + e^{-}_{CB}) \quad (3)$$

$$ZnV@Ag^{*}\left(h^{+}_{VB}\right) + H_2O \rightarrow H^{+} + {}^{\bullet}OH \quad (4)$$

$$ZnV@Ag^{*}\left(e^{-}_{CB}\right) + H^{+} \rightarrow 1/2H_2 \quad (5)$$

$${}^{\bullet}OH + \text{Lactic acid} \rightarrow H_2O + CO_2 \quad (6)$$

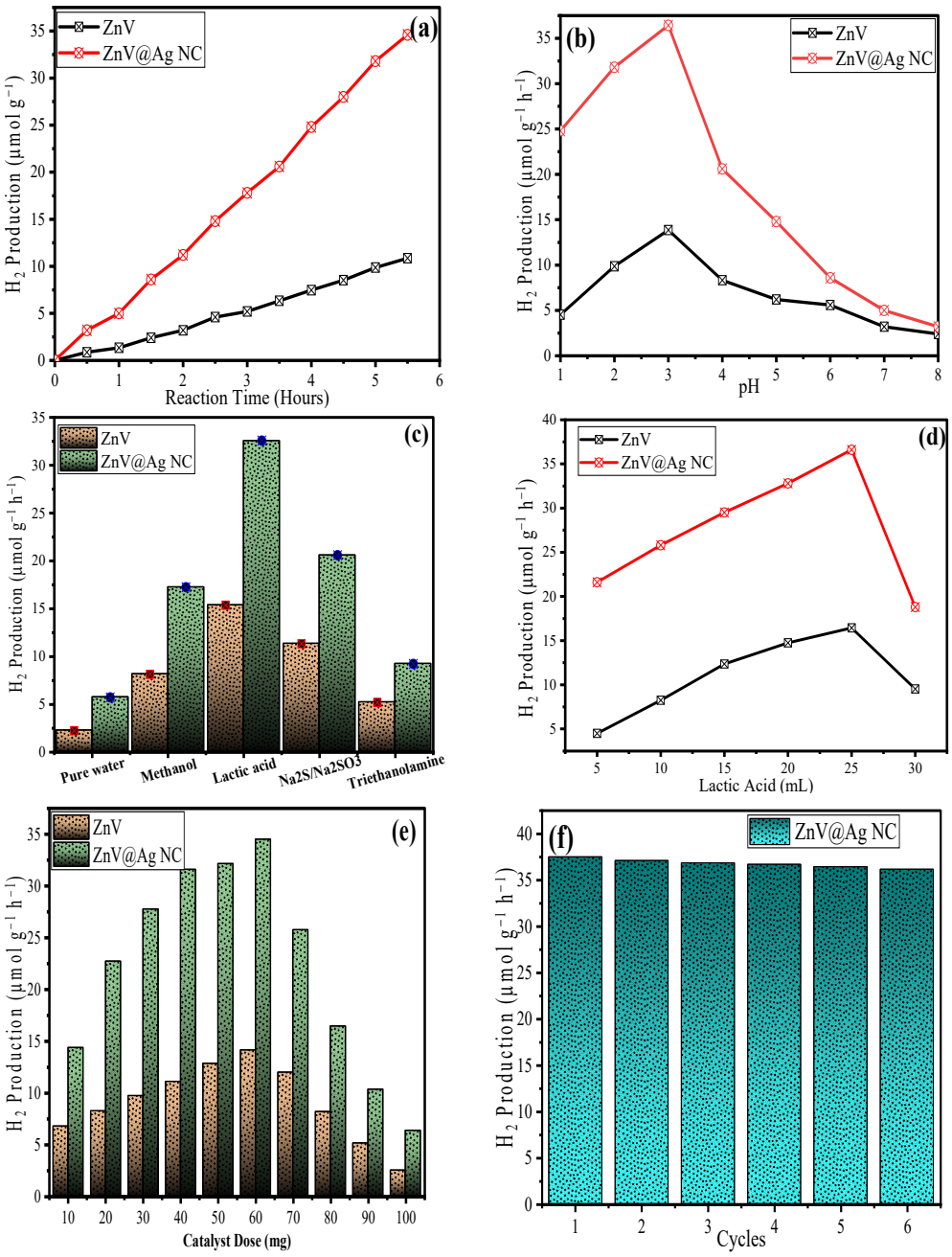

Figure 8. Photocatalytic H_2 generation activities of ZnV and ZnV@Ag NC at different times (**a**), pH values (**b**), and solvents (**c**). Photocatalytic H_2 generation activities of ZnV and ZnV@Ag NC with different doses of catalyst (**d**) and lactic acid (**e**). Stability study of ZnV@Ag NC for H_2 production (**f**).

Table 2. H_2 production activities of **ZnV and** ZnV@Ag NC.

Photocatalyst Materials	H_2 Production Efficiency	Light Source
ZnV@Ag NC	37.52 μmolg^{-1}h^{-1}	Xenon lamp (λ = 420 nm)
ZnV	16.44 μmolg^{-1}h^{-1}	Xenon lamp (λ = 420 nm)

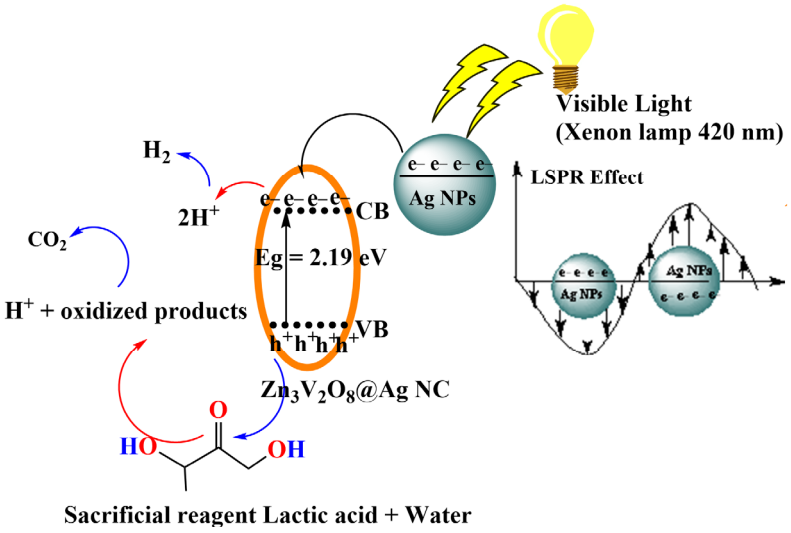

Scheme 1. Illustration of H_2 gas production by ZnV@Ag NC using lactic acid as sacrificial reagent.

3. Experimental Section

3.1. Chemicals and Reagents

Zinc nitrate (Zn $(NO_3)_2$.4H2O, 99%), vanadium pentoxide (V_2O_5, 99.99%), and silver nitrate ($AgNO_3$, >98%) were purchased from Merck, Germany. Hydrogen peroxide (30%, H_2O_2), sodium hydroxide (NaOH pellets, 98%), and ethanol (C_2H_5OH, 99%) were supplied by Loba Chemie, Mumbai, India. All of the chemicals were used as received without further purification.

3.2. Synthesis of $Zn_3V_2O_8$/Ag NPs

We adopted a benign approach for the preparation of $Zn_3V_2O_8$/Ag NPs and $Zn_3V_2O_8$ [28]. In a 100 mL capacity beaker, 0.75 g of V_2O_5 dissolved in 20 mL of DI water was added, followed by the addition of 30% H_2O_2 drop by drop. The color of the solution changed from bright yellow to orange. Amounts of 0.25 g of Zn $(NO_3)_2.6H_2O$ and 0.12g of $AgNO_3$ in 30 mL of DI water were added to the above solution and mixed under magnetic stirring for 60 min. After 60 min, a 0.5 M solution of NaOH (20 mL) was added to the above mixture to maintain a pH of 8–9. The mixture was transferred to a 100 mL Teflon-lined autoclave and heated at 185 °C for 24 h. After the completion of the reaction, the autoclave was allowed to naturally cool at room temperature, and the precipitate was collected by centrifugation. The material was washed several times with DI water and ethanol to remove any unreacted reactant species, dried at 80 °C for 5 h in a hot air oven, and finally calcined at 600 °C for 3 h at a heating rate of 5 °C/min. Similarly, pristine ZnV was also prepared by the same method but without using $AgNO_3$. In further studies, $Zn_3V_2O_8$ and the $Zn_3V_2O_8$/Ag nanocomposite are labeled as ZnV and ZnV@Ag NC.

3.3. H_2 Production Assembly

Hydrogen production experiments were carried out in a photocatalytic reactor using a 350 W Xenon lamp with a cutoff wavelength of 420 nm and an intensity of 180 mW cm^{-2} as a visible-light source. The synthesized ZnV and ZnV@Ag NC materials were immersed in a solution of lactic acid/water as a sacrificial agent and placed in a photocatalytic reactor equipped with a double-walled quartz reaction vessel connected to a closed gas circuit with

a water jack flushing cold water to maintain the temperature of the reaction at 10 °C. The produced H_2 gas was analyzed using a multichannel analyzer (Emerson) equipped with a thermal conductivity detector. Scheme 2 presents the schematic diagram of photocatalytic hydrogen production.

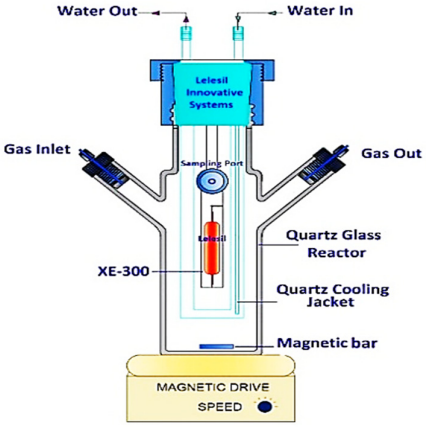

Scheme 2. Schematic diagram of a photocatalytic hydrogen production reactor.

3.4. Apparatus

In the present study, a Rigaku (Rigaku Ultima IV, Austin, TX, USA) powder X-ray diffractometer (XRD) was utilized for recording XRD patterns. A Zeiss (Zeiss Gemini SEM, Carl Zeiss, Jena, Germany) microscope was used to capture the field-emission scanning electron microscopy (FESEM) images of the prepared materials. A Thermo-Scientific instrument (K-alpha, MA USA) was used to obtain the X-ray photoelectron spectroscopy (XPS) spectra of the synthesized materials. The ultraviolet–visible (UV-vis) spectra were recorded on an Agilent Cary Instrument (Cary 60, Santa Clara, CA, USA). Energy-dispersive X-ray spectroscopic (EDX) studies were performed on an Oxford EDX instrument connected to SEM. Transmission electron microscopy (TEM) images of the obtained samples were collected on a Tecnai G2, F30 instrument (Netherlands). Photocatalytic H_2 production studies were performed on a Joel gas chromatograph. Fourier transform infrared (FTIR) spectra of the samples were obtained on a BRUKER spectrometer (Alpha II, Billerica, MA, USA).

4. Conclusions

In the present study, a facile synthesis was employed for the preparation of ZnV and a ZnV@Ag nanocomposite. The physiochemical and optical properties of the prepared ZnV and ZnV@Ag NC were evaluated by utilizing various advanced techniques. The optical band gap of ZnV was reduced from 2.33 eV to 2.19 eV with the introduction of Ag NPs to the ZnV matrix/surface. This indicates that ZnV@Ag NC, with a narrow band gap of 2.19 eV, will absorb light, and improved photocatalytic H_2 production can be observed. The excellent H_2 amount of 37.52 $\mu molg^{-1}h^{-1}$ was obtained using ZnV@Ag NC as a photocatalyst compared to ZnV. ZnV@Ag NC also showed excellent cyclic stability, which can be attributed to the presence of electroactive sites and a better ion/electron transport path in the prepared ZnV@Ag NC with improved conductivity. This study proposes a new eco-friendly and cost-effective photocatalyst for photocatalytic H_2 production applications.

Author Contributions: Conceptualization, F.A.A. and I.H.; Methodology, F.A.A. and I.H.; Software, H.S.A. and I.H.; Validation, H.S.A. and I.H.; Formal analysis, A.S.A. and H.K.A.; Investigation, A.S.A. and H.K.A.; Resources, A.S.A. and H.K.A.; Data curation, I.H.; Writing—original draft, A.S.A.; Writing—review & editing, I.H.; Visualization, H.S.A.; Supervision, F.A.A. and H.S.A.; Project administration, F.A.A.; Funding acquisition, F.A.A. All authors have read and agreed to the published version of the manuscript.

Funding: This work was funded by deputyship of Research and Innovation, Ministry of Education in Saudi Arabia, project number IFK-SURG-2-1326.

Data Availability Statement: Data is contained within the article.

Acknowledgments: The authors extend their appreciation to the deputyship of Research and Innovation, Ministry of Education in Saudi Arabia, for funding this research. All the authors have consented to the acknowledgment.

Conflicts of Interest: The authors declare that there is no conflict of interest related to this research.

References

1. Ishaq, H.; Dincer, I.; Crawford, C. A review on hydrogen production and utilization: Challenges and opportunities. *Int. J. Hydrogen Energy* **2022**, *47*, 26238–26264. [CrossRef]
2. Ahmad, K.; Mobin, S.M. Recent Progress and Challenges in $A_3Sb_2X_9$-Based Perovskite Solar Cells. *ACS Omega* **2020**, *5*, 28404–28412. [CrossRef]
3. Alam, M.W.; Al Qahtani, H.S.; Souayeh, B.; Ahmed, W.; Albalawi, H.; Farhan, M.; Abuzir, A.; Naeem, S. Novel Copper-Zinc-Manganese Ternary Metal Oxide Nanocomposite as Heterogeneous Catalyst for Glucose Sensor and Antibacterial Activity. *Antioxidants* **2022**, *11*, 1064. [CrossRef]
4. Ahmad, K.; Shinde, M.A.; Song, G.; Kim, H. Design and fabrication of $MoSe_2/WO_3$ thin films for the construction of electrochromic devices on indium tin oxide based glass and flexible substrates. *Ceram. Int.* **2021**, *47*, 34297–34306. [CrossRef]
5. Alam, M.W.; Azam, H.; Khalid, N.R.; Naeem, S.; Hussain, M.K.; BaQais, A.; Farhan, M.; Souayeh, B.; Zaidi, N.; Khan, K. Enhanced Photocatalytic Performance of Ag_3PO_4/Mn-ZnO Nanocomposite for the Degradation of Tetracycline Hydrochloride. *Crystals* **2022**, *12*, 1156. [CrossRef]
6. Suresh Philip, C.; Nivetha, A.; Sakthivel, C.; Veena, C.G.; Prabha, I. Novel fabrication of cellulose sprinkled crystalline nanocomposites using economical fibrous sources: High performance, compatible catalytic and electrochemical properties. *Microporous Mesoporous Mater.* **2021**, *318*, 111021. [CrossRef]
7. Ahmad, K.; Shinde, M.A.; Kim, H. Molybdenum disulfide/reduced graphene oxide: Progress in synthesis and electro-catalytic properties for electrochemical sensing and dye sensitized solar cells. *Microchem. J.* **2021**, *169*, 106583. [CrossRef]
8. Low, W.H.; Khiew, P.S.; Lim, S.S.; Siong, C.W.; Chia, C.H.; Ezeigwe, E.R. Facile synthesis of graphene-$Zn_3V_2O_8$ nanocomposite as a high performance electrode material for symmetric supercapacitor. *J. Alloys Compd.* **2019**, *784*, 847–858. [CrossRef]
9. Liu, W.; Wang, X.; Yu, H.; Yu, J. Direct Photoinduced Synthesis of Amorphous $CoMoS_x$ Cocatalyst and Its Improved Photocatalytic H_2-Evolution Activity of CdS. *ACS Sustain. Chem. Eng.* **2018**, *6*, 12436–12445. [CrossRef]
10. Sharma, R.; Almáši, M.; Nehra, S.P.; Rao, V.S.; Panchal, P.; Paul, D.R.; Jain, I.P.; Sharma, A. Photocatalytic hydrogen production using graphitic carbon nitride (GCN): A precise review. *Renew. Sustain. Energy Rev.* **2022**, *168*, 112776. [CrossRef]
11. Fujishima, A.; Honda, K. Electrochemical Photolysis of Water at a Semiconductor Electrode. *Nature* **1972**, *238*, 37–38. [CrossRef] [PubMed]
12. Shanmugaratnam, S.; Velauthapillai, D.; Ravirajan, P.; Christy, A.A.; Shivatharsiny, Y. CoS_2/TiO_2 Nanocomposites for Hydrogen Production under UV Irradiation. *Materials* **2019**, *12*, 3882. [CrossRef] [PubMed]
13. Sekar, K.; Kassam, A.; Bai, Y.; Coulson, B.; Li, W.; Douthwaite, R.E.; Sasaki, K.; Lee, A.F. Hierarchical bismuth vanadate/reduced graphene oxide composite photocatalyst for hydrogen evolution and bisphenol A degradation. *Appl. Mater. Today* **2021**, *22*, 100963. [CrossRef]
14. Dhabarde, N.; Carrillo-Ceja, O.; Tian, S.; Xiong, G.; Raja, K.; Subramanian, V.R. Bismuth Vanadate Encapsulated with Reduced Graphene Oxide: A Nanocomposite for Optimized Photocatalytic Hydrogen Peroxide Generation. *J. Phys. Chem. C* **2021**, *125*, 23669–23679. [CrossRef]
15. Marberger, A.; Ferri, D.; Elsener, M.; Sagar, A.; Artner, C.; Schermanz, K.; Kröcher, O. Relationship between structures and activities of supported metal vanadates for the selective catalytic reduction of NO by NH_3. *Appl. Catal. B Environ.* **2017**, *218*, 731–742. [CrossRef]
16. Lashari, N.R.; Zhao, M.; Zheng, Q.; Gong, H.; Duan, W.; Xu, T.; Wang, F.; Song, X. Excellent cycling stability and capability of novel mixed-metal vanadate coated with V_2O_5 materials in an aqueous solution. *Electrochim. Acta* **2019**, *314*, 115–123. [CrossRef]
17. Vignesh, K.; Hariharan, R.; Rajarajan, M.; Suganthi, A. Visible light assisted photocatalytic activity of TiO_2–metal vanadate (M = Sr, Ag and Cd) nanocomposites. *Mater. Sci. Semicond. Process.* **2013**, *16*, 1521–1530. [CrossRef]
18. Muthurasu, A.; Tiwari, A.P.; Chhetri, K.; Dahal, B.; Kim, H.Y. Construction of iron doped cobalt-vanadate-cobalt oxide with metal-organic framework oriented nanoflakes for portable rechargeable zinc-air batteries powered total water splitting. *Nano Energy* **2021**, *88*, 106238. [CrossRef]
19. Zhang, W.; Zhang, Y.; Yuan, H.; Li, J.; Ding, L.; Chu, S.; Wang, L.; Zhai, W.; Jiao, Z. Carbon hollow matrix anchored by isolated transition metal atoms serving as a single atom cocatalyst to facilitate the water oxidation kinetics of bismuth vanadate. *J. Colloid Interface Sci.* **2022**, *616*, 631–640. [CrossRef]
20. Yao, X.; Zhao, X.; Hu, J.; Xie, H.; Wang, D.; Cao, X.; Zhang, Z.; Huang, Y.; Chen, Z.; Sritharan, T. The Self-Passivation Mechanism in Degradation of $BiVO_4$ Photoanode. *IScience* **2019**, *19*, 976–985. [CrossRef]
21. Su, J.; Bai, Z.; Huang, B.; Quan, X.; Chen, G. Unique three dimensional architecture using a metal-free semiconductor cross-linked bismuth vanadate for efficient photoelectrochemical water oxidation. *Nano Energy* **2016**, *24*, 148–157. [CrossRef]

22. Rajaji, U.; Govindasamy, M.; Sha, R.; Alshgari, R.A.; Juang, R.-S.; Liu, T.-Y. Surface engineering of 3D spinel $Zn_3V_2O_8$ wrapped on sulfur doped graphitic nitride composites: Investigation on the dual role of electrocatalyst for simultaneous detection of antibiotic drugs in biological fluids. *Compos. Part B Eng.* **2022**, *242*, 110017. [CrossRef]
23. Yin, Z.; Qin, J.; Wang, W.; Cao, M. Rationally designed hollow precursor-derived $Zn_3V_2O_8$ nanocages as a high-performance anode material for lithium-ion batteries. *Nano Energy* **2017**, *31*, 367–376. [CrossRef]
24. Rajkumar, S.; Elanthamilan, E.; Princy Merlin, J. Facile synthesis of $Zn_3V_2O_8$ nanostructured material and its enhanced supercapacitive performance. *J. Alloys Compd.* **2021**, *861*, 157939. [CrossRef]
25. Gan, L.; Deng, D.; Zhang, Y.; Li, G.; Wang, X.; Jiang, L.; Wang, C. $Zn_3V_2O_8$ hexagon nanosheets: A high-performance anode material for lithium-ion batteries. *J. Mater. Chem. A* **2013**, *2*, 2461–2466. [CrossRef]
26. Mirsadeghi, S.; Ghoreishian, S.M.; Zandavar, H.; Behjatmanesh-Ardakani, R.; Naghian, E.; Ghoreishian, M.; Mehrani, A.; Abdolhoseinpoor, N.; Ganjali, M.R.; Huh, Y.S.; et al. In-depth insight into the photocatalytic and electrocatalytic mechanisms of $Mg_3V_2O_8$@$Zn_3V_2O_8$@ZnO ternary heterostructure toward linezolid: Experimental and DFT studies. *J. Environ. Chem. Eng.* **2023**, *11*, 109106. [CrossRef]
27. Khan, F.U.; Chen, Y.; Khan, Z.U.H.; Khan, A.U.; Ahmad, A.; Tahir, K.; Wang, L.; Khan, M.R.; Wan, P. Antioxidant and catalytic applications of silver nanoparticles using Dimocarpus longan seed extract as a reducing and stabilizing agent. *J. Photochem. Photobiol. B Biol.* **2016**, *164*, 344–351. [CrossRef]
28. Liu, P.; Yi, J.; Bao, R.; Fang, D. A flower-like $Zn_3V_2O_8$/Ag composite with enhanced visible light driven photocatalytic activity: The triple-functional roles of Ag nanoparticles. *New J. Chem.* **2019**, *43*, 7482–7490. [CrossRef]
29. Scherrer, P. Estimation of the Size and Internal Structure of Colloidal Particles by Means of Rontgen Rays. *Nachr. Von Der Ges. Der Wiss. Zu Göttingen* **1918**, *26*, 98–100.
30. Luo, J.; Ning, X.; Zhan, L.; Zhou, X. Facile construction of a fascinating Z-scheme AgI/$Zn_3V_2O_8$ photocatalyst for the photocatalytic degradation of tetracycline under visible light irradiation. *Sep. Purif. Technol.* **2021**, *255*, 117691. [CrossRef]
31. Jiang, Y.H.; Liu, P.P.; Tian, S.J.; Liu, Y.; Peng, Z.Y.; Li, F.; Ni, L.; Liu, Z.C. Sustainable visible-light-driven Z-scheme porous $Zn_3(VO_4)_2$/g-C_3N_4 heterostructure toward highly photoredox pollutant and mechanism insight. *J. Taiwan Inst. Chem. Eng.* **2017**, *78*, 517–529. [CrossRef]
32. Pei, L.Z.; Lin, N.; Wei, T.; Liu, H.D.; Yu, H.Y. Zinc Vanadate Nanorods and Their Visible Light Photocatalytic Activity. *J. Alloys Compd.* **2015**, *631*, 90–98. [CrossRef]
33. Ahmed, N.; Mukhtar, S.; Gao, W.; Zafar Ilyas, S. Ab-Initio Calculations of Structural, Electronic, and Optical Properties of $Zn_3(VO_4)_2$. *Chin. Phys. B* **2018**, *27*, 033101. [CrossRef]
34. Du, M.; Xiong, S.; Wu, T.; Zhao, D.; Zhang, Q.; Fan, Z.; Zeng, Y.; Ji, F.; He, Q.; Xu, X. Preparation of a Microspherical Silver-Reduced Graphene Oxide-Bismuth Vanadate Composite and Evaluation of Its Photocatalytic Activity. *Materials* **2016**, *9*, 160. [CrossRef]
35. Ijaz, M. Plasmonic Hot Electrons: Potential Candidates for Improved Photocatalytic Hydrogen Production. *Int J. Hydrogen Energy* **2022**. [CrossRef]
36. Arif Sher Shah, M.S.; Zhang, K.; Park, A.R.; Kim, K.S.; Park, N.G.; Park, J.H.; Yoo, P.J. Single-Step Solvothermal Synthesis of Mesoporous Ag–TiO_2–Reduced Graphene Oxide Ternary Composites with Enhanced Photocatalytic Activity. *Nanoscale* **2013**, *5*, 5093–5101. [CrossRef] [PubMed]
37. Kubelka, P. Ein Beitrag Zur Optik Der Farbanstriche (Contribution to the Optic of Paint). *Z. Fur Tech. Phys.* **1931**, *12*, 593–601.
38. Kondarides, D.I.; Daskalaki, V.M.; Patsoura, A.; Verykios, X.E. Hydrogen Production by Photo-Induced Reforming of Biomass Components and Derivatives at Ambient Conditions. *Catal. Lett.* **2008**, *122*, 26–32. [CrossRef]
39. Wang, Y.; Liu, T.; Tian, W.; Zhang, Y.; Shan, P.; Chen, Y.; Wei, W.; Yuan, H.; Cui, H. Mechanism for Hydrogen Evolution from Water Splitting Based on a MoS_2/WSe_2 Heterojunction Photocatalyst: A First-Principle Study. *RSC Adv.* **2020**, *10*, 41127–41136. [CrossRef]